# The nature of the *fiber* noise with the FOCES spectrograph

## Nature, modeling and a way to achieve *S/N* > 400

### F. Grupp[★]

Universitäts Sternwarte München, Scheinerstr. 1, 12345 München, Germany

**Abstract.** The non-white noise noticed using the fiber-fed FOCES spectrograph is recognized as the result of vignetting to an uneven distribution of monochromatic light in the spectrograph beam behind the fiber exit. This phenomenon – that can be assigned to *every* fiber-coupled spectrograph with vignetting of the light path behind the fiber – is qualitatively and quantitatively described and modeled. The $S/N$ ratio that seemed to be limited to $\approx 200$ when surrounding the object exposure by two flatfield exposures is shown to reach the theoretical limit (defined by the linear range of the CCD-detector) of $S/N \approx 500$. This is achieved by using multiple flatfield exposures in combination with a *fiber vibration device* allowing non-harmonic movement of the fiber during exposure time.

**Key words.** instrumentation: spectrographs – techniques: spectroscopic – telescopes

## 1. Introduction

Medium and high resolution spectroscopy has become a preeminent tool in answering astrophysical questions and probing astrophysical models and theories. The enormous wavelength stability and the large spectral coverage of echelle spectrographs that are coupled via an optical fiber to the telescope's focus allows highly accurate work in many fields of astrophysics using even small and medium-type telescopes. For example radial velocity determinations (see for example Liu et al. 1991), stellar parameter work (see for example Fuhrmann et al. 1997; Baumueller & Gehren 1997; Mashonkina et al. 1999) and numourous other investigations can be carried out at telescopes of 1 . . . 2.5 m type.

FOCES, the **f**iber **o**ptical **c**oupled **e**chelle **s**pectrograph at CENTRO ASTRONOMICO HISPANO ALEMAN on top of the Calar Alto, Spain was built and installed at the 2.2 m telescope there. For a description of the FOCES layout and optical properties see Pfeiffer et al. (1998).

When the first scientific test observations with FOCES were carried out a limitation of the signal-to-noise ratio ($S/N$) to $\approx 200$ was noticed (see Fig. 1). This limitation in $S/N$ gave severe restrictions to the spectrograph performance and is documented by Pfeiffer et al. (1998) and Fuhrmann et al. (1997).

In his efforts to understand these restrictions Fuhrmann (1998) showed that the non-white noise detected was related to the telescope movement. In fact it did not occur in test exposures where the guiding of the telescopewas stopped, and the noise got worse with larger telescope movements. Due to the
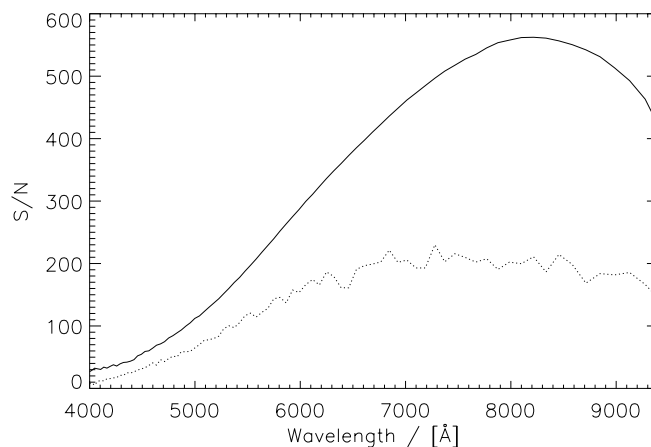
---

**Fig. 1.** Measured and predicted signal to noise. Upper full curve: Expected photon noise; lower dotted curve: Measured noise.

mechanically stable design of the telescope module and the mechanical decoupling of the spectrograph itself which is standing one floor beneath the telescope, this noise was blamed on the movement of the optical fiber connecting telescope and spectrograph, and named *fiber noise*.

Framing each object exposure with flatfield exposures taken directly before and after object integration, and calibrating the object frame using solely those two framing calibrations for flatfield correction, Fuhrmann reached $S/N \approx 250$.

Although $S/N \approx 200$ is good for many scientific purposes it is very unsatisfying for high resolution (up to $\Delta\lambda/\lambda = 60\,000$) stellar parameter and chemistry work. In addition it results in

**Table 1.** Spectrograph settings.

| Date | CCD | Slit width | Diaphragm | $\Delta\lambda/\lambda$ |
|------|-----|-----------|-----------|------------------------|
| May 99 | Lor#11i | $120\,\mu$ | $200\,\mu$ | 60 000 |
| June 99 | Site#1d | $130\,\mu$ | $300\,\mu$ | 42 000 |
| Sept. 99 | Site#1d | $130\,\mu$ | $300\,\mu$ | 42 000 |
| Dec. 99 | Lor#11i | $110\,\mu$ | $200\,\mu$ | 64 000 |

a loss of 30% of usable observing time as flat field exposures have to be taken right before and after every object exposure.

We use the knowledge about the modal distribution of monochromatic light after transmission through optical fibers to show the nature of this noise and show ways of achieving full signal to noise without losing time in taking flat field exposures during the astronomical night.

Baudrand et al. (1998) noted that the modal distribution of light leaving the fiber exit together with vignetting leads to an additional noise in high-resolution spectra of fiber-fed spectrographs. Further investigations of Baudrand & Walker (2001) do not cover this type of noise, but another, yet not understood type of noise occurring even if spacial filtering is omitted[1]. Furthermore the effect described by Baudrand & Walker (2001) is on a 3 times higher level as far as $S/N$ is concerned. While they measure a limitation on $S/N \approx 450$ at $\lambda = 9500$ Å our spectra are limited to $S/N \approx 150$ in this spectral region.

Therefore we first describe a method for the accurate measurement of the fiber noise in Sect. 2. Afterwards the distribution of light after being transferred through an optical fiber is described and shown in Sect. 3, followed by the presentation of a model describing the measured noise. This model is then compared with our observations. Section 4 gives a short discussion of these results and states some rules for spectrograph setup in order to minimize the fiber noise. In addition we briefly discuss the results of Baudrand & Walker (2001). Finally we show a method of avoiding this noise and achieving full $S/N$ in Sect. 5. The procedure described there is in use at Calar Alto observatory since early 1999 in several experimental states and confirms the results of Baudrand & Walker (2001) who developed some similar device. Differences to their approach will also be discussed in Sect. 5.

## 2. Observations, tests and measuring the noise

### 2.1. Observations

The observations and test exposures were obtained during an observation run in June 1999 and in a special test session during FOCES commissioning time in September 1999 on the 2.2 m telescope of the Calar Alto Observatory. The Lunar spectra presented were obtained by Klaus Fuhrmann during a proceeding observation run in May 1999. Table 1 shows the observational data and spectrograph settings for these observations.

---

[1] "...we carefully avoided any vignetting between the fiber output and the CCD to prevent spatial filtering of modes emerging from the fiber". Baudrand & Walker (2001).
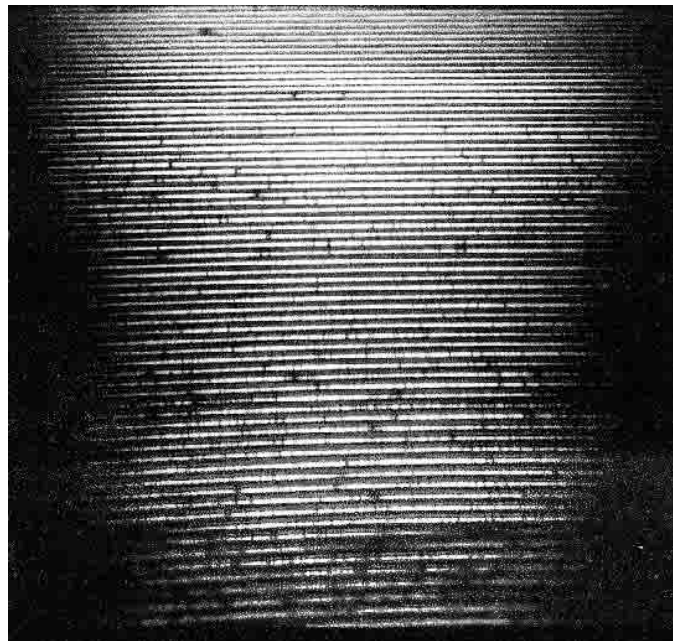


**Fig. 2.** Echelle image on CCD.
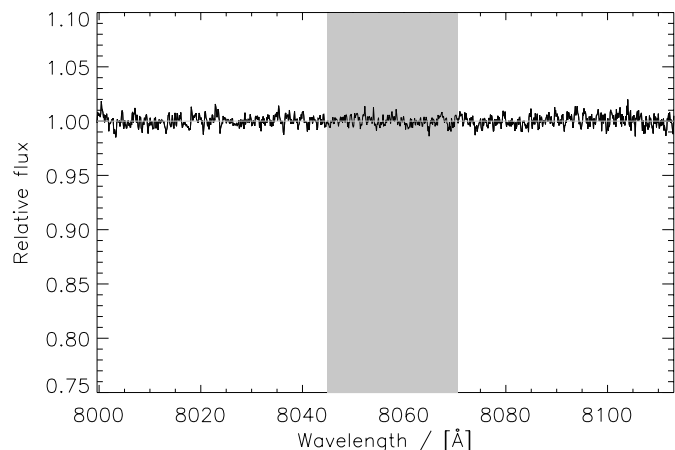


**Fig. 3.** One order of the extracted flat field spectrum.

### 2.2. Noise measurement

Figure 2 shows an image of the FOCES *echelle order pattern spectrum* observed with the Calar Alto Site#1d CCD. In order to measure the noise introduced by the fiber movement a flatfield exposure (looked at as a spectrum) is reduced using a flatfield exposure (looked at as a flatfield) of the same integration time, but taken at a different telescope, thus fiber position. This results in a spectrum free of absorption lines. As shown in Fig. 3 for one spectral order these spectra are indeed *flat*. The total spectral noise $\bar{\sigma}$ is measured in each order by taking a sample of 250 points in the order center and calculating their standard deviation.

Dividing this noise by the mean flux of this sample leads to the *measured $S/N$*. Finally each measured $S/N$ – value is assigned the central wavelength of the range it was calculated from. The shaded range in Fig. 3 shows the range where the noise measurement calculation was performed.
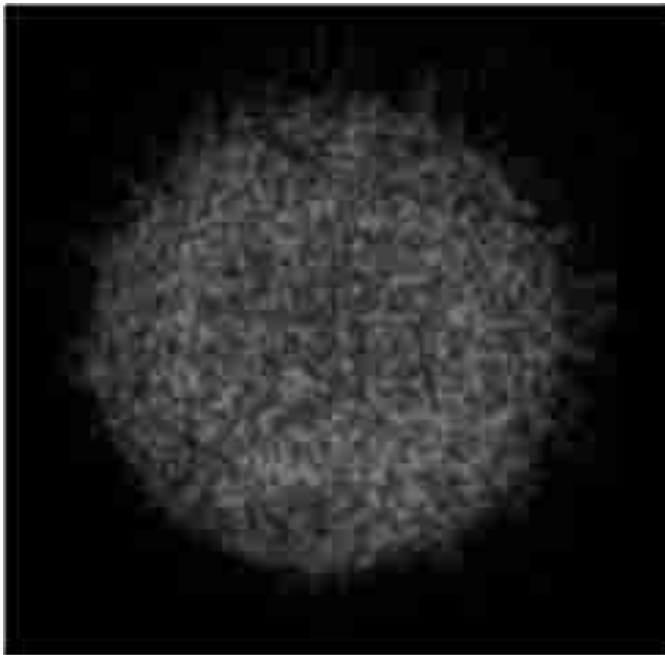
**Fig. 4.** Speckle distribution behind a test fiber system.

## 3. Fiber modes and a statistical model of the noise

Before we start developing a model for the noise found with the spectrograph we will look at the distribution of monochromatic light after passing an optical fiber.

### 3.1. The fiber modes

The propagation of monochromatic light through a long, thin fiber fed with evenly distributed light leads to a non-uniform distribution of light at the fiber exit[2]. As shown by Sharma et al. (1981) the number of speckles or modes at the fiber end depends on the diameter of the fiber $r$, the $f$-ratio the fiber is fed with $\frac{\#}{f}$ and the wavelength $\lambda$:

$$M = 2\pi^2 \left(\frac{r}{\lambda}\right)^2 \sin^2\left(\arctan\left(1/\left(2\frac{\#}{f}\right)\right)\right). \tag{1}$$

Figure 4 shows the speckle distribution at the exit of a test fiber used with the FOCES spectrograph. The fiber was fed with a HeNe-laser of 660 nm wavelength through a microlens input system.

Due to the coupling of the FOCES fiber to the telescope's cassegrain focus (see Pfeiffer et al. 1998, for a brief description of the fiber feeding geometry) the input $f$-ratio depends solely on the diameter of the entrance diaphragm preceding the fiber input micro-lens system. For all three available entrance apertures and at seven wavelengths we present the number of modes found at the fiber exit in Table 2.

It is of great importance to point out here that the detailed distribution of modes at the fiber exit depends strongly on spatial assembly and bending of the 20-meter-long fiber. Slight

---

[2] It should be pointed out that this speckle distribution at the fiber end is not an effect of degrading and occurs in unbent, unstressed fibers.

**Table 2.** Number of modes for different wavelengths and entrance diaphragm diameters.

| Diaphragm | 130 $\mu$ | 200 $\mu$ | 300 $\mu$ |
|---|---|---|---|
| #/$f$ | 8 | 5 | 2.7 |
| 3000 Å | 8534 | 21 715 | 72 722 |
| 4000 Å | 4800 | 12 215 | 40 906 |
| 5000 Å | 3072 | 7818 | 26 180 |
| 6000 Å | 2134 | 5429 | 18 180 |
| 7000 Å | 1567 | 3989 | 13 357 |
| 8000 Å | 1200 | 3054 | 10 226 |
| 9000 Å | 978 | 2413 | 8080 |
| Wavelength | | # of modes | |

changes in bending and positioning of the fiber, far below the limit where degrading would occur, as evoked by even small changes in telescope position due to guiding, lead to enormous changes of the speckle pattern at the fiber exit.

### 3.2. Vignetting of the beam

The $f$-ratio of the beam leaving the fiber depends on entrance $f$-ratio and degrading.

$$\left(\frac{\#}{f}\right)_{\text{out}} \geq \left(\frac{\#}{f}\right)_{\text{in}}. \tag{2}$$

Fiber feed and fiber casing are constructed in a way to prevent any stress and sharp bending of the fiber. (All FOCES fibers are covered by a Teflon tube surrounded by steel netting.) Therefore we assume that for the moderate $f$-ratios ($2.7 \cdots 8.0$) of FOCES fiber operation no significant degrading occurs. This means conservation of the input $f$-ratio at the fiber exit.

We again refer to Pfeiffer et al. (1998) for details concerning the optical layout and just state here that the light cone leaving the micro-lens at the fiber exit is vignetted by the spectrograph entrance slit for high resolution ($\Delta\lambda/\lambda = 40\,000 \cdots 60\,000$) and large ($>150\,\mu$m) entrance diaphragms.

The area $S_v$ of the beam that is vignetted by an entrance slit of $x\,\mu$m in the focal plane of a fiber fed with an entrance diaphragm of $R\,\mu$m can be expressed by simple geometrical considerations.

$$S_v = R^2 \left(2\arccos\left(\frac{x}{R}\right) - \sin\left(2\arccos\left(\frac{x}{R}\right)\right)\right). \tag{3}$$

We define the unvignetted fraction of light passing through the spectrograph's entrance slit by:

$$g = \frac{\pi R^2 - S_v}{\pi R^2}$$
$$= 1 - \frac{1}{\pi}\left(2\arccos\left(\frac{x}{R}\right) - \sin\left(2\arccos\left(\frac{x}{R}\right)\right)\right). \tag{4}$$

The latter equation is represented in Table 3 for the most commonly used assemblies for diaphragm and slit width of the FOCES spectrograph.

A second source of vignetting that can be assigned to the FOCES spectrograph is related to the *overfilling* of the optical grating. Although less important, Fig. 5 shows that the grid is overfilled by about 5% of the beam's surface.

**Table 3.** Fraction $g$ of light cone cut by an entrance slit of 110 $\mu$, 130 $\mu$ and 150 $\mu$ respectively for different entrance diaphragms.

| Diaphragm | 130 $\mu$ | 200 $\mu$ | 300 $\mu$ |
|---|---|---|---|
| Fraction for slit width 110 $\mu$ | 0.93 | 0.66 | 0.46 |
| Fraction for slit width 130 $\mu$ | 1.00 | 0.73 | 0.53 |
| Fraction for slit width 150 $\mu$ | 1.00 | 0.86 | 0.61 |
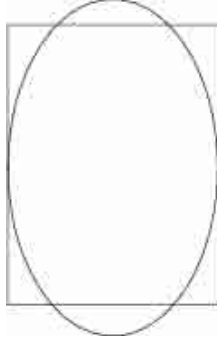


**Fig. 5.** Overfilling of the diffraction grating by the beam.

## 3.3. Statistical model of the fiber noise

As noted first by Baudrand et al. (1998) the movement of fiber modes with the movement of the fiber itself together with vignetting of the beam may lead to fiber noise.

In order to quantify this effect and allow predictions we have to make a few assumptions.

– *Even distribution of speckles*. It is assumed that the modal speckles are equally distributed over the fiber exit and therefore over the fiber exit image on the spectrographs entrance slit. Figure 4 shows that this assumption is justified.
– *Homogeneous intensity of the modes of one wavelength*. In addition to the latter we assume equally distributed intensity of all modal speckles over the fiber exit and (after imaging by the micro-lens) over the speckle images in the focal plane.
– *Stationarity of the modal distribution during single flat field exposures*. We assume the modal picture to be unchanged on time scales of flat field exposing. Because we turned off the telescope guiding and allowed some relaxation time before taking flat field exposures of 3.5 and 10 s, this assumption is well justified.
– *Statistically independent speckle distribution for different telescope positions*. We assume the distribution of speckles to change completely, and in a statistical manner, when changing the telescope position by a significant angular distance. Simple tests with the laser illuminated fiber show that a fiber movement of less than 2 cm changes the speckle picture completely. Because it is impossible to reproduce the exact fiber position when moving the telescope to different positions this assumption holds true.
– *Only entrance slit vignetting*. Due to the large fraction of light cut by the entrance slit and the comparatively low fraction cut by overfilling the grating we assume that all vignetting can be assigned to the entrance slit. The second

source of vignetting would (if not neglegible) result in a higher noise in the model described below.
– *2 pixel resolution element*. FOCES is designed to image the entrance slit on a resolution element of two pixel elongation in the dispersion direction. This should be accounted for when comparing calculated and measured $S/N$.

Using the assumptions and simplifications described above we are able to build a simple but powerful model of *fiber noise*.

For a given geometric assembly of telescope and fiber, this means fixed $f$-ratio $\#/f$, slit width $x$ and fiber diameter $r$, we are able to assign $M$ spectral modes to a given wavelength $\lambda$ (see Table 2).

Due to vignetting not all $M = M_{r,\#/f}(\lambda)$ modes reach the spectrograph camera and CCD detector. A significant fraction of modes is taken out of the light path by the entrance slit cutting the beam in the focal plane of the fiber exit lens (see Table 3).

Using these assumptions the mean number of modes reaching the CCD is given by

$$\hat{M} = Mg. \tag{5}$$

Changing the modal distribution by changing the fiber position, will lead to a statistical noise $\sigma$ caused by modes getting into and out of the vignetted area. This is a statistical problem described by the *binomial distribution* with a standard deviation $\sigma = \sqrt{V}$ with $V = Mg(1 - g)$ the variance of the binomial distribution, leading to

$$\sigma = \sqrt{M \cdot g \cdot (1 - g)}. \tag{6}$$

Under the assumptions mentioned the number of unvignetted, monochromatic modes entering the spectrograph corresponds directly to the number of photons reaching the CCD. Dividing the *noise* $\sigma$, calculated in (6) by the number of unvignetted modes $\hat{M}$ we get a measurable value. This *noise per signal* becomes:

$$\bar{\sigma} = \frac{\sigma}{\hat{M}} = \frac{1}{\sqrt{M}} \sqrt{\frac{1 - g}{g}}. \tag{7}$$

We choose this description of *noise per signal* instead of the commonly used *signal per noise* to illustrate and check its simple dependency on wavelength. Taking into account Eq. (1) we get:

$$\bar{\sigma} \sim \lambda \tag{8}$$

i.e. the measurable value $\bar{\sigma}$ depends only on the (known) geometry of the spectrograph feeding optics and the wavelength $\lambda$.

## 3.4. Checking the model

For a FOCES configuration with the 300 $\mu$ (200 $\mu$ respectively) entrance diaphragm, leading to $\#/f = 2.7$ (5.0) at the fiber entrance together with a spectrograph slit of 150 $\mu$ (110 $\mu$) we get from this geometry a fraction of the unvignetted beam $g = 0.61$ ($g = 0.66$) – see also Table 1.
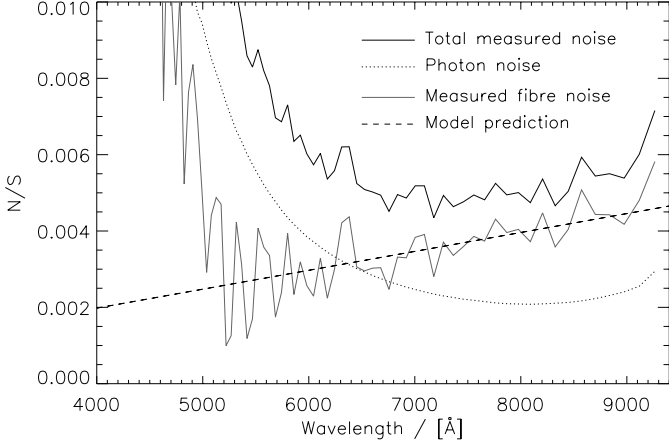
**Fig. 6.** Measured and predicted noise. Upper full curve: total measured noise; lower dotted curve: photon noise; full grey curve: measured fiber noise; dashed black line: model prediction.

Using Eq. (1) we get:

$$M_{x=150,R=300,\#/f=2.7}(\lambda) = 6.55 \times 10^{-9} \times \frac{1}{\lambda^2} \qquad (9)$$

$$M_{x=110,R=200,\#/f=5.0}(\lambda) = 1.95 \times 10^{-9} \times \frac{1}{\lambda^2}.$$

This leads to a functional dependency of noise per signal with $\lambda$ given by

$$\bar{\sigma}_{x=150,R=300,\#/f=2.7}(\lambda) = 0.98 \times 10^{-6} \times \lambda \left[ \text{Å} \right] \qquad (10)$$

$$\bar{\sigma}_{x=110,R=200,\#/f=5.0}(\lambda) = 1.63 \times 10^{-6} \times \lambda \left[ \text{Å} \right].$$

It is now possible to check the measured noise (evaluated as described in Sect. 2.2 against the calculated noise emerging from our model. In order to account for the "smearing out" of spectral information to a two pixel element, we have to correct the $N/S$ data from Eq. (10) by $1/\sqrt{2}$.

The pure fiber noise is evaluated from our measurements by subtracting photon noise from total noise according to:

$$\sigma_{\text{fiber}} = \sqrt{\sigma_{\text{measured}}^2 - \sigma_{\text{photon}}^2}. \qquad (11)$$

We present the results in Fig 6. Here the measured total noise over 88 spectral orders reaching from 3900 Å to 9400 Å is plotted in the uppermost full line curve. The expected photon noise is shown as a dotted curve below. Note that photon noise would allow a $S/N \approx 500$ around $\lambda = 7000$ Å, because the readout noise of cooled CCD-detectors can be neglected. Using Eq. (11) the measured fiber noise is displayed as a grey curve. Finally the straight black line represents our model's predictions. *Measurement and prediction are in good agreement* as long as we keep to spectra of a certain minimum quality. Below $S/N \approx 100$, Fig. 6 shows stronger fiber noise than predicted by our model. This is due to the fact that Eq. (11) only holds true for large numbers. As soon as we are down to only a few hundred photons per resolution element we cannot expect Eq. (11) to allow a realistic calculation of $\sigma_{\text{fiber}}$.
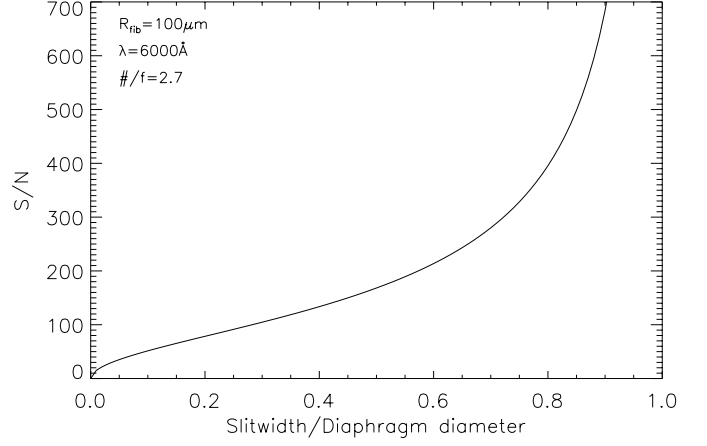


**Fig. 7.** Signal to noise dependency on the fraction of slit width and input aperture diameter.

## 4. Discussion

As shown in Sect. 3 the propagation of light through optical fibers together with beam vignetting in the spectrograph behind the fiber exit leads to fiber noise.

This fiber noise can be predicted using the knowledge of the geometry of the light cone coupling into the fiber, the fiber diameter and the fraction of vignetting in the light path of the spectrograph.

### 4.1. Spectrograph setup

The following considerations are carried out choosing a typical FOCES setting. For a practical reason the observer will be interested in how to adjust the spectrograph, namely slitwidth and entrance aperture in order to obtain good results. Figure 7 shows this dependency. It is apparent that large slit width and small diaphragm diameter leads to less vignetting and therefore low fiber noise. Large diaphragm together with narrow entrance slit leads to large vignetting and therefore increased fiber noise.

If $f$-ratio and diaphragm diameter are not independent, the previous analysis should be repeated, looking at the influence of the entrance aperture's diameter on a constant, resolution-determined slit width. We choose a slit width of 150 $\mu$m corresponding to $\lambda/\Delta\lambda = 42\,000$. In Fig. 8 we plot the influence of the entrance diaphragm's diameter on $S/N$, considering both its influence on the $f$-ratio and on the ratio slit with to entrance aperture.

As FOCES in its $\lambda/\Delta\lambda = 42\,000$ setting is optimized to the 200 $\mu$m diaphragm we conclude from this figure that, from the point of fiber noise, using a larger diaphragm does not degrade the noise very much. Nevertheless, throughput limitation for good seeing conditions (see Pfeiffer et al. 1998, Fig. 7) puts a strong limitation on observing quality.

### 4.2. A short note on the Baudrand results

The effect described by Baudrand & Walker (2001) will be briefly discussed at the end of this section. Their detailed very-
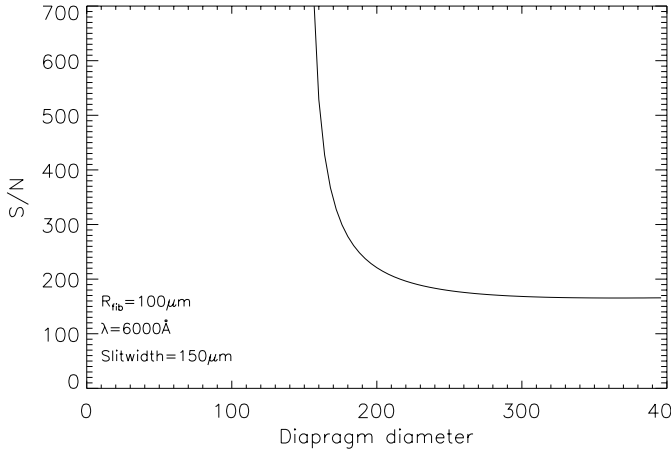
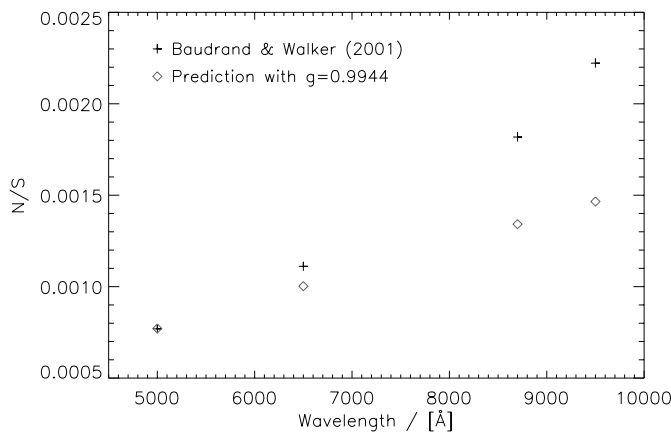**Fig. 8.** Signal to noise dependenc on full input aperture treatment.



**Fig. 9.** Baudrand data and a plot of our quantitative model with a vignetting of $g = 0.9944$.

high signal to noise work shows a limitation of $S/N$ to values >450 in the visual part of the spectrum.

This implies that there is almost no vignetting within the light-path between fiber exit and CCD-camera. Figure 9 shows the data given by Baudrand & Walker (2001) translated to our $N/S$ plot as black crosses. The second set of data plotted in Fig. 9 is our model in which a fraction of 0.56% of the light path is assumed to suffer vignetting. This very small fraction could easily be explained as light lost at the grating or the image slicer. Including this artificial assumption, only a small but measurable remainder of the noise ($S/N_{rest} > 1500$) could be blamed on processes other than pure vignetting.

## 5. Removing noise restrictions. How to achieve full *S/N*

After having modeled and analyzed the nature and dependencies of the *fiber noise* we will now show a way of removing this type of noise and its restrictions to spectral quality. Figure 10 shows the theoretical photon noise expected for a well exposed flat field "spectrum".

To allow observations to reach such a high signal-to-noise ratio we have to compensate *fiber noise*. This can be achieved using two technical "tricks".
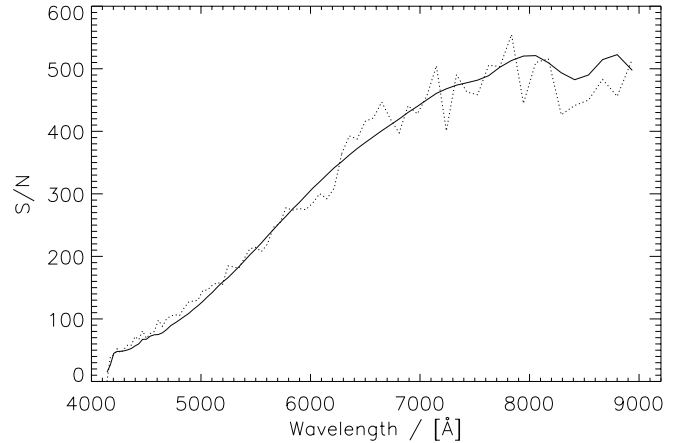


**Fig. 10.** Signal to noise data for flat field exposure as it would be expected from pure photon statistics (full line) and measured $S/N$ for moved fiber (dotted line).

1. The fiber is moved in a non-harmonic, i.e chaotic way. We introduce a *fiber-shaking device* between telescope module and spectrograph. Due to its double pendulum-like assembly the harmonic movement of the primary motion is turned into chaotic motion. This movement, that is set to be fast compared to the guiding movement of the telescope and the image exposure time, leads to extreme and quick changes of the speckle distribution on the fiber exit. During an exposure we can subdivide the speckle information into a very large number of single speckle distributions. This large number of different speckle subimages makes it possible to consider the integrated spectral information as an average of all sub-distributions. As the number is large, the mean is well defined in a statistical sense and noise is effectively suppressed.
2. Flat-field division is not done by a single frame, fiber-noise contaminated due to its short exposure, but by the average of $n$ frames. Again the noise introduced by flatfielding is reduced due to the coadding of the spectral information in these frames.

Figure 10 shows the measured $S/N$ ratio (dotted line) for a flat field "spectrum" with moved fiber and 10 flat fields used. The expected photon noise limitation is reached by using the techniques explained above.

Concerning the results of Baudrand & Walker (2001) our tests do not confirm any dependence of the result on the frequency of the movement. This might be due to the fact that our device works in a double pendulum-like, chaotic mode. In fact the frequency we use to manipulate the fiber on a length of $\approx 2.5$ m in length is only $\approx 1$ Hz, the amplitude rises up to $\approx 0.5$ m.

## References

Baudrand, J., Guinouard, I., & Jocou, L. 1998, in ASP Conf. Ser., 152

Baudrand, J., & Walker, G. A. H. 2001, PASP, 113, 851

Baumueller, D., & Gehren, T. 1997, A&A, 325, 1088

Fuhrmann, K. 1998, Private communication

Fuhrmann, K., Pfeiffer, M., Frank, C., Reetz, J., & Gehren, T. 1997, A&A, 323, 909

Liu, T., Janes, K. A., & Bania, T. M. 1991, ApJ, 377, 141

Mashonkina, L., Gehren, T., & Bikmaev, I. 1999, A&A, 343, 519

Pfeiffer, M. J., Frank, C., Baumueller, D., Fuhrmann, K., & Gehren, T. 1998, A&AS, 130, 381

Sharma, A. B., Halme, S. J., & Butusow, M. M. 1981, Optical Fibre Systems and Their Components (Springer Verlag)